Supporting Information

to

Nanostructuring niobium oxides using polymer-grafted cellulose nanocrystals and nanofibers as sacrificial scaffolds

Yen Theng Cheng,[1,2] Sandya S. Athukoralalage,[3] Nasim Amiralian,[3] Chris D. Ling,[2,4] Markus Müllner[1,2,]*

[1]Key Centre for Polymers and Colloids, School of Chemistry, The University of Sydney, Sydney, NSW 2006, Australia; [2]The University of Sydney Nano Institute (Sydney Nano), Sydney, NSW 2006, Australia; [3]Australian Institute of Bioengineering and Nanotechnology (AIBN), The University of Queensland, 4072 St Lucia, Queensland, Australia; [4]School of Chemistry, The University of Sydney, Sydney, NSW 2006, Australia.

Email correspondence to markus.muellner@sydney.edu.au

Table of Contents

Materials

Materials

Sugarcane trash was provided by Sunshine Sugar, Australia. Sodium hydroxide (99%) was sourced from Chem-supply. Sulphuric acid was sourced from RCI Labscan. Cellulose nanocrystals (CelluRods^{TM}) was purchased from CelluForce Inc. Glacial acetic acid, ethyl *α*-bromoisobutyrate (EB*i*B), *α*-bromoisobutyryl bromide (*α*-BiBB), copper(I) chloride, triethylamine and 4-dimethylaminopyridine (DMAP) were purchased from Merck. Deuterated chloroform (CDCl3, 99%) was sourced from Cambridge Isotopes Laboratories. Hydrochloric acid (analytical grade, 32%) was sourced from AJAX Fine Chem. Sodium chlorite (technical grade, 80 %), ammonium niobate(V) oxalate hydrate (NbOxA), 2-dimethylamino)ethyl methacrylate (DMAEMA, 98%), N,N,N′,N″,N″-pentamethyldiethylenetriamine (PMDETA, 99%) were purchased from Sigma Aldrich. DMAEMA monomer was purified by passing through a column of neutral aluminium oxide for inhibitor removal. NbOxA was freeze-dried and stored in a hot oven to remove excess moisture prior to the complexation process. All remaining chemicals were used as received.

Methods

Fourier-transform infrared spectroscopy (FTIR) measurements. All pristine, surface-modified, polymer-grafted cellulose nanocrystals (CNC) and cellulose nanofibers (CNF) were analyzed using a PerkinElmer Spectrum Two FTIR spectrometer. All spectra were recorded from 4000 to 400 cm^{-1} with a spectral resolution of 1 cm^{-1} and 16 scans.

Proton nuclear magnetic resonance (^{1}H NMR) spectra were recorded in $CDCl_3$ using a 300 MHz Bruker Avance system at 300 K.

Size exclusion chromatography (SEC). SEC was performed using a Shimadzu Prominence UFLC (ultra-fast liquid chromatography) system fitted with a Shim-pack GPC-800DP guard column followed by two in-series Phenogel columns (5 μm, 104 Å and 105 Å). The system eluent was HPLC grade dimethyl acetamide (DMAc) containing LiBr (0.03 wt%) and BHT

(each at 0.05 wt%), eluting at a flow rate of 1 mL/min. The column assembly was incubated at 50 °C, and retention times were calibrated using PMMA narrow standards from PSS. Sacrificial PDMAEMA SEC samples were passed through passed through a 220 nm nylon filter several times prior to injection to remove residual CNC-*g*-PDMAEMA or CNF-*g*-PDMAEMA.

Thermogravimetric analysis (TGA) was performed on a TA Instruments Discovery thermogravimetric analyzer. Solid samples were heated under a flow of air from room temperature to 600 ºC at a ramp rate of 4 ºC min^{-1}. The samples were held at 100 ºC for 30 min to remove residual solvent.

Scanning electron microscopy (SEM) was performed on a Zeiss Sigma HD FEG SEM. Images were collected at a working distance of 3.5–5.0 mm at an accelerating voltage of 3 kV. All SEM samples were sputtered with gold (5 nm) prior to imaging.

Transmission electron microscopy (TEM) was performed on a JEM-2100CR instrument equipped with a 5k × 4k CMOS camera (EMSIS). Images were collected in bright-field mode with a spot size of 1 with diffraction contrast enhanced by using an objective lens with an aperture size of 20 μm, at an accelerating voltage of 200 kV. All materials were well-dispersed in water (10 mg/mL) and drop-casted onto an ultrathin carbon film that was supported by a copper grid.

Powder X-ray diffraction (PXRD) data were collected on a PANalaytical X-pert Pro powder diffractometer, with non-monochromated Cu K_a X-ray radiation (λ = 1.5406 Å) and a PIXcel1D detector in continuous scanning mode at a speed of 1.26º min^{-1} and a step size of 0.001º over the 2θ angle range 5–80º. Average crystallite sizes were estimated using Debye-Scherrer equation.

Ultraviolet (UV) irradiation for Rhodamine B degradation was performed on The RAYONET reactor Model RPR-100 with sixteen 14W light bulbs (254 nm). The Rhodamine solutions were stirred continuously throughout the irradiation.

UV-Vis absorbance spectra were recorded using a Horiba Duetta spectrofluorometer with a temperature control enabled (25 ºC) using 10 mm quartz cuvettes. All spectra were collected from 400 – 700 nm, with a step increment of 1 nm, an integration time of 0.04 s and a band pass of 2 nm.

Supporting Results

S1. TEM of pristine CNC and CNF

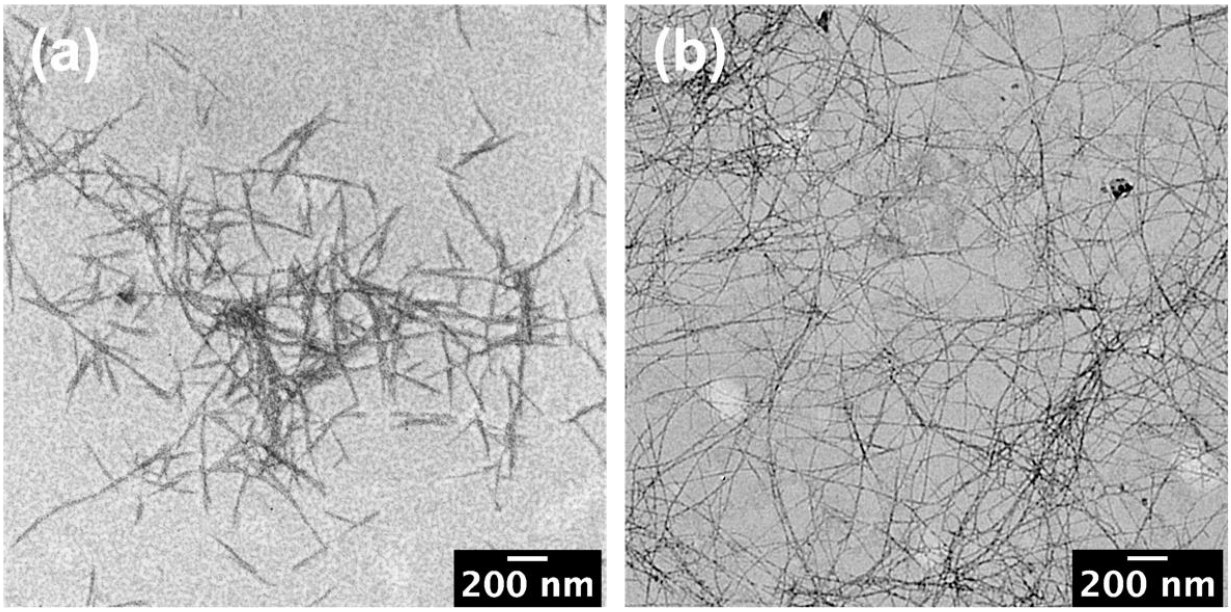

Figure S1. SEM micrographs of (a) pristine CNC and (b) pristine CNF.

S2. Polymerisation kinetics of SI-ATRP of DMAEMA from CNC-Br and CNF-Br

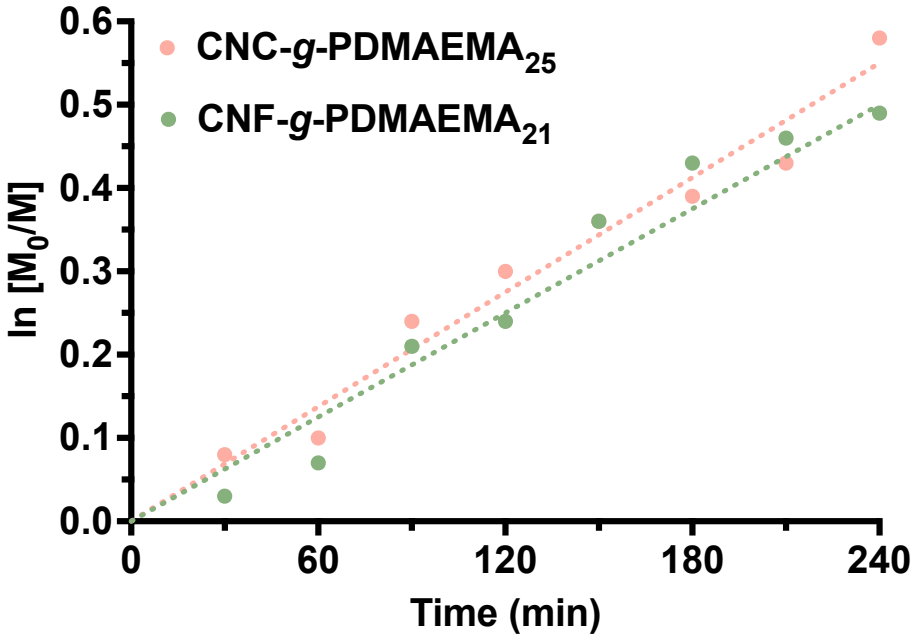

Figure S2. First-order kinetic plot for the SI-ATRP of DMAEMA from CNC-Br and CNF-Br polyinitiators monitored by ^{1}H NMR spectroscopy.

S3. SEC of sacrificial PDMAEMA

PDMAEMA was polymerised from CNC-Br and CNF-Br in the presence of a sacrificial initiator (EBiB). The resultant sacrificial PDMAEMA was analysed using SEC.

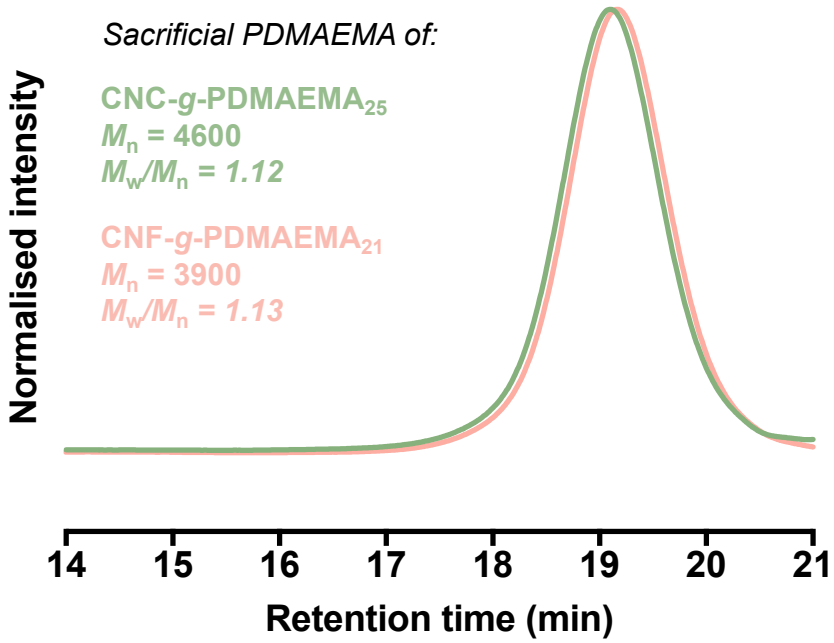

Figure S3. SEC of sacrificial PDMAEMA measured using DMac as the eluent.

S4. SEM of *nc*-NbOxA and *nf*-NbOxA hybrids

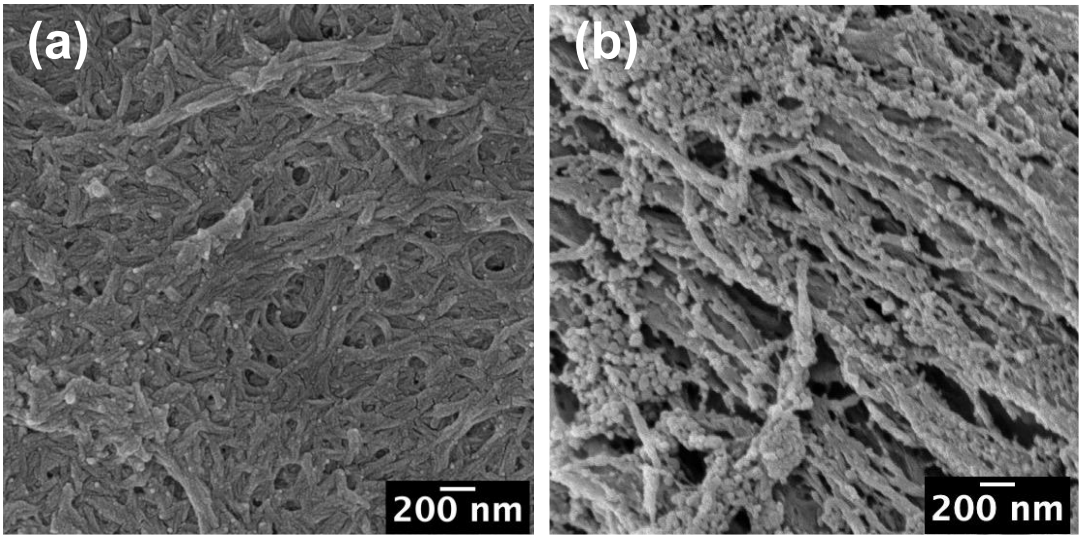

Figure S4. SEM micrographs of (a) *nc*-NbOxA and (b) *nf*-NbOxA.

S5. TGA curves of CNC-*g*-PDMAEMA$_{25}$ and CNF-*g*-PDMAEMA$_{21}$

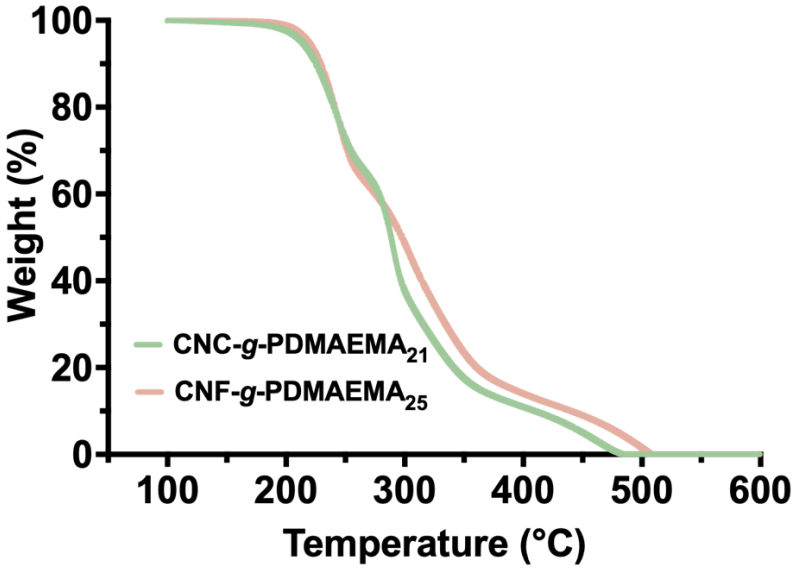

Figure S5. TGA curves of CNC-*g*-PDMAEMA$_{25}$ and CNF-*g*-PDMAEMA$_{21}$ showing their complete thermal degradation after 500 ºC.

S6. SEM and PXRD of *nc*-Nb_2O_5-1100 and *nf*-Nb_2O_5-1100 heated for 2 hours

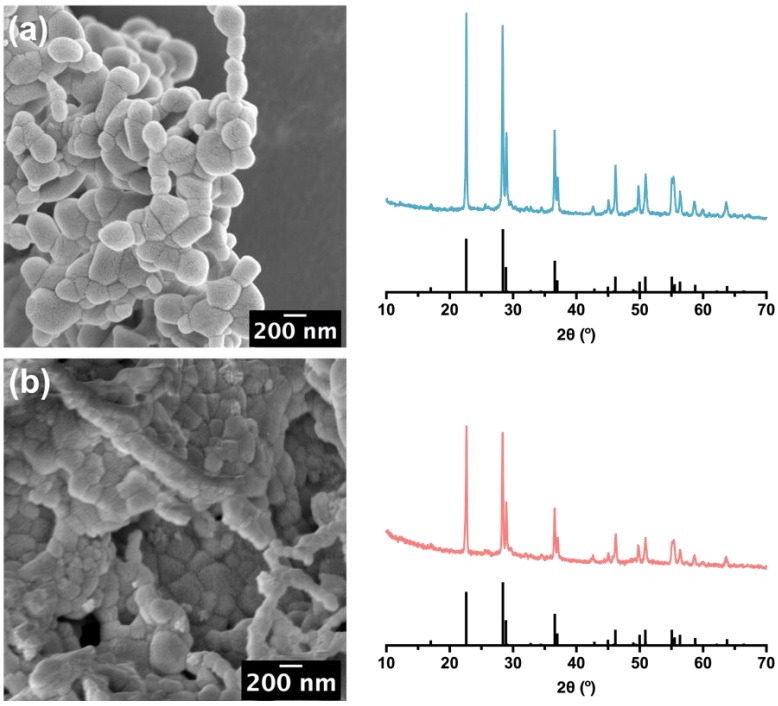

Figure S6. SEM micrographs and PXRD data (Cu K$_\alpha$, λ = 1.5406 Å) of (a) *nc*-Nb_2O_5-1100 and (b) *nf*-Nb_2O_5-1100 heated for 2 hours. The reference Bragg diffraction peaks of the orthorhombic Nb_2O_5 crystalline phase are shown at the bottom of each plot.

S7. SEM of Nb_2O_5 synthesized with and without nanocellulose polymer brush templates.

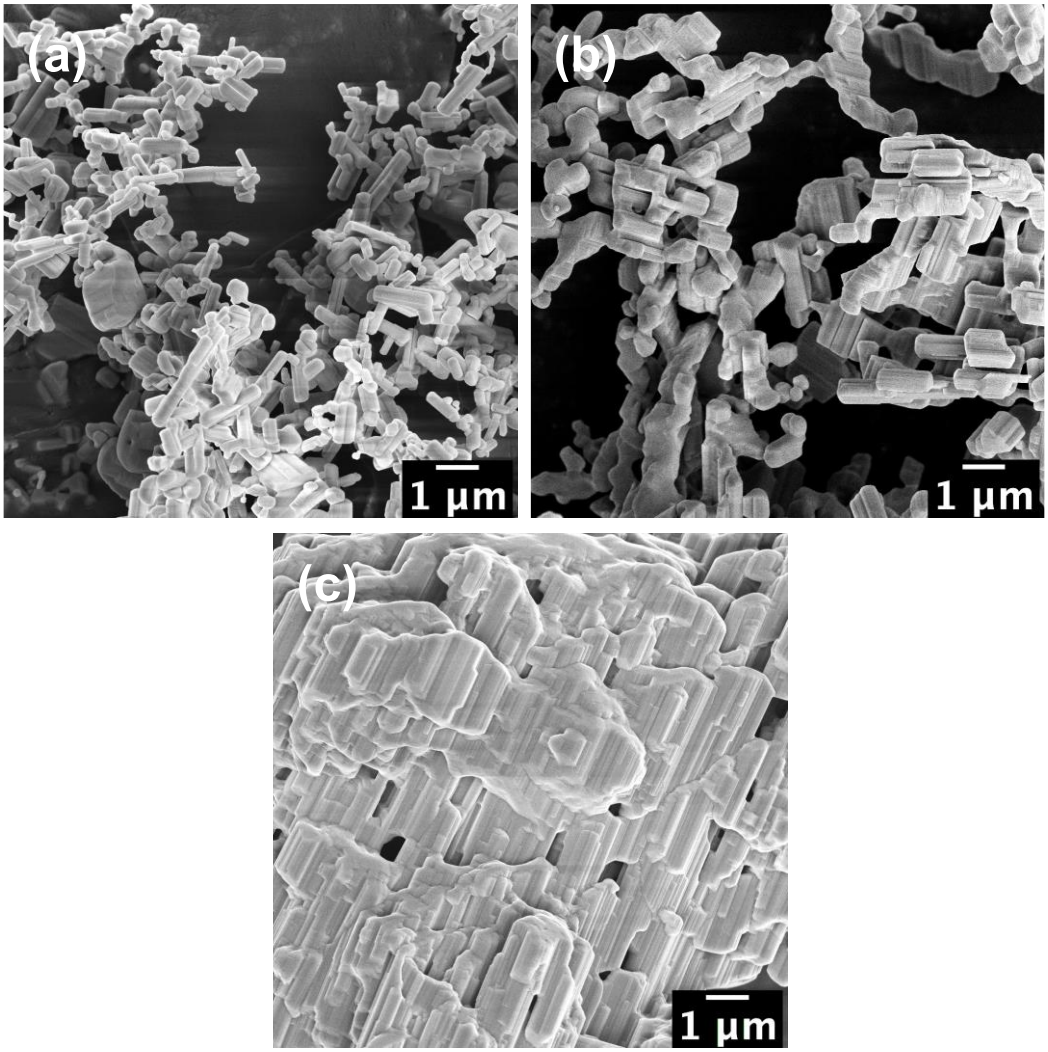

Figure S7. SEM micrographs of monoclinic (a) *nc*-Nb_2O_5-1100, (b) *nf*-Nb_2O_5-1100 and (c) non-templated Nb_2O_5 showing their morphological difference.

S8. Absorbance changes of Rhodamine B with no catalyst and bulk Nb_2O_5 prepared at 550 ºC

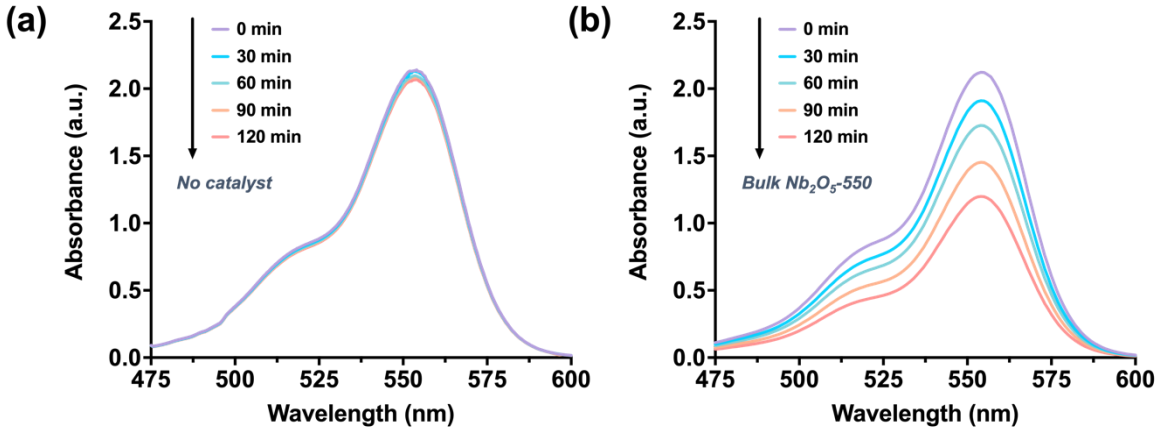

Figure S8. Absorbance changes of Rhodamine B solutions under UV-C irradiation with (a) no catalyst added and (b) bulk Nb_2O_5.

S9. Comparison of Rhodamine B degradation solutions.

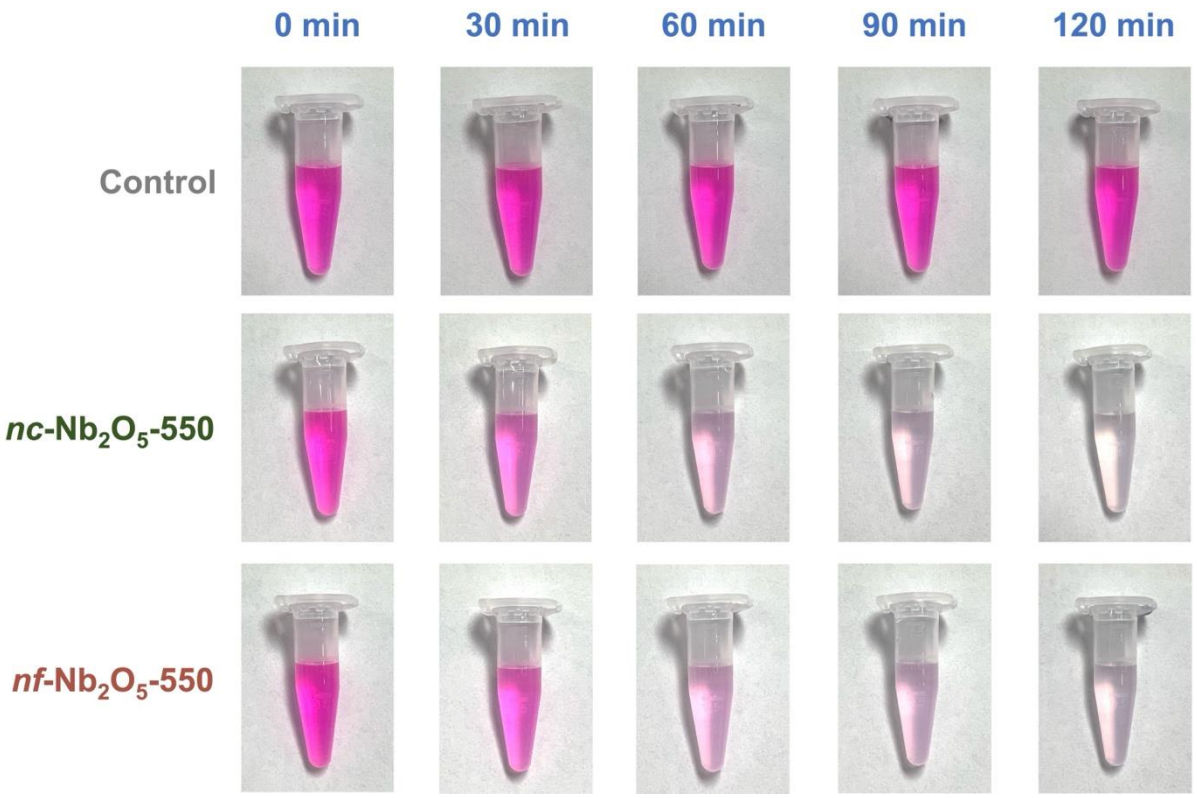

Figure S9. Digital photographs showing the colour change of the Rhodamine B solutions containing no catalyst, *nc*-Nb_2O_5-550 and *nf*-Nb_2O_5-550.

S10. Comparison of Rhodamine B degradation efficiencies between the solutions with *nc*-Nb_2O_5 and *nf*-Nb_2O_5 prepared at different temperatures.

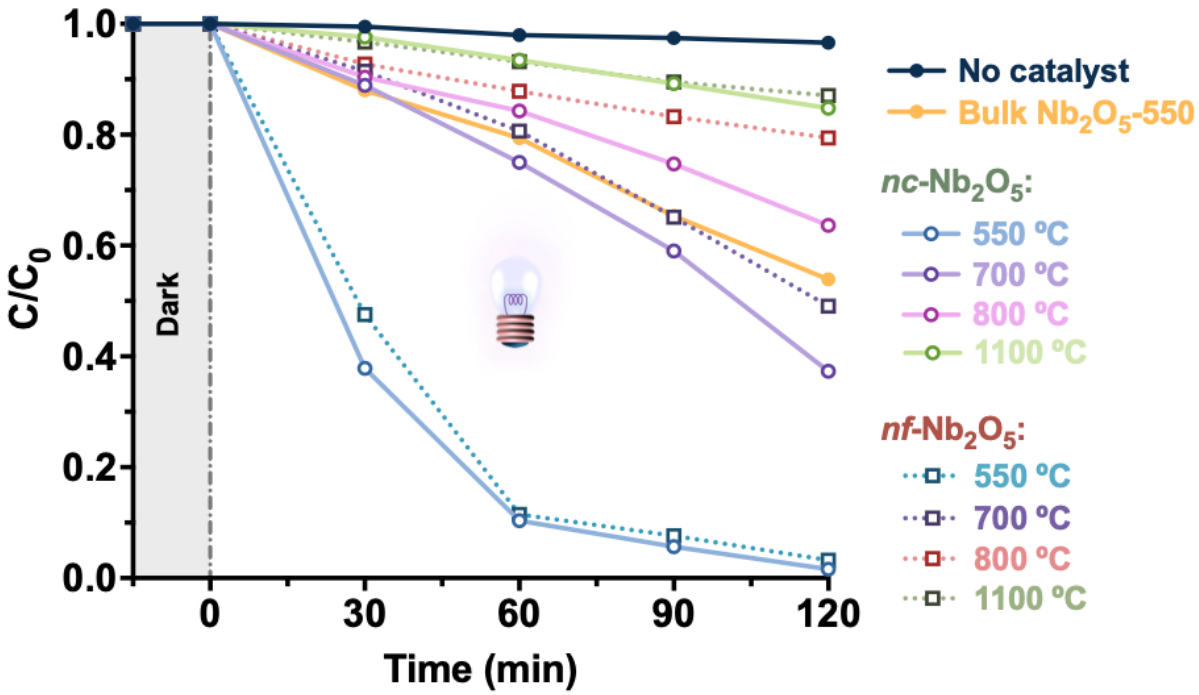

Figure S10. Change of Rhodamine B concentration as a function of time for solutions with different *nc*-Nb_2O_5 or *nf*-Nb_2O_5 samples, and solution with no catalyst (control) and solution with bulk Nb_2O_5-550.